NASA

Technical Memorandum 79714

Impact of Short Interval SMS Digital Data on Wind Vector Determination for a Severe Local Storms Area

Cynthia A. Peslen

FEBRUARY 1979

National Aeronautics and Space Administration

Goddard Space Flight Center
Greenbelt, Maryland 20771

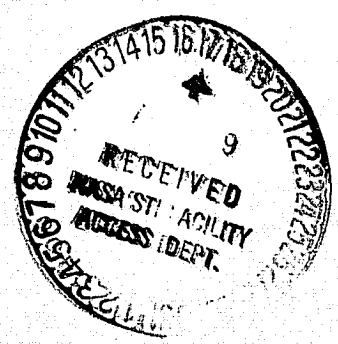

TM 79714

IMPACT OF SHORT INTERVAL SMS DIGITAL DATA ON WIND VECTOR DETERMINATION FOR A SEVERE LOCAL STORMS AREA

Cynthia A. Peslen

Goddard Laboratory for Atmospheric Sciences

NASA/Goddard Space Flight Center

Greenbelt, MD 20771

February 1979

GODDARD SPACE FLIGHT CENTER
Greenbelt, Maryland

IMPACT OF SHORT INTERVAL SMS DIGITAL DATA ON WIND VECTOR DETERMINATION FOR A SEVERE LOCAL STORMS AREA

Cynthia A. Peslen
Goddard Laboratory for Atmospheric Sciences
NASA/Goddard Space Flight Center
Greenbelt, MD 20771

ABSTRACT

The impact of 5 minute interval SMS-2 visible digital image data in analyzing severe local storms is examined using wind vectors derived from cloud tracking on time lapsed sequences of geosynchronous satellite images. The cloud tracking areas are located in the Central Plains, where on 6 May 1975, hail-producing thunderstorms occurred ahead of a well defined dry line.

Cloud tracking is performed on the Goddard Space Flight Center Atmospheric and Oceanographic Information Processing System (AOIPS). Lower tropospheric cumulus tracers are selected with the assistance of a cloud top height algorithm. Divergence is derived from the cloud motions using a modified Cressman (1959) objective analysis technique which is designed to organize irregularly spaced wind vectors into uniformly gridded wind fields.

The results demonstrate that satellite-derived wind vectors and their associated divergence fields complement conventional meteorological analyses in describing the conditions preceding severe local storm development. For this case, an apparent area of convergence consistently appeared ahead of the dry line and coincided with the developing area of severe weather. The magnitude of the maximum convergence varied between 10^{-5} sec^{-1} to 10^{-4} sec^{-1}. The number of satellite-derived wind vectors which were required to describe the kinematic properties of the low level atmosphere was adequate before numerous cumulonimbus cells formed. This technique is limited in areas of advanced convection.

CONTENTS

ILLUSTRATIONS

ILLUSTRATIONS (Continued)

TABLES

IMPACT OF SHORT INTERVAL SMS DIGITAL DATA ON WIND VECTOR DETERMINATION FOR A SEVERE LOCAL STORMS AREA

1. Introduction

Cloud tracking on geosynchronous satellite images to derive kinematic properties of severe local storms is based on the assumption that cloud motions approximate the environmental winds. The best low level tracers appear to be cumulus turrets (0.5–3.0km diameters) using brightness centers as the tracking point (Fujita et al., 1975). A cloud will not move precisely with the environmental wind because it's motions are affected by entrainment, vertical wind shear, and it's own vertical development. However, previous studies have shown that a level exists whereby cloud motions approximate environmental winds. An earlier study by Hubert and Whitney (1971) compared ATS-1 and ATS-3 cloud motions with rawinsonde winds and determined that a level of best fit (LBF) existed for their sampled low clouds between 0.9km and 1.5km. The median vector deviation between the cloud motions and rawinsonde winds was 4.6msec^{-1} for 600 low cloud tracers.

A number of studies have been done to compare aircraft-measured winds and cloud motions. Wagner and Telford (1976) measured air motion in and near small cumuli over land using the NCAR Buffalo aircraft inertial navigation system. The results showed that cloud motions corresponded very closely with the magnitude and direction of the wind in the sub cloud layer. For three clouds, differences of 0.8msec^{-1}, 0.6msec^{-1}, and 1.5msec^{-1} were found between the cloud drift relative to the ground and the embedding wind below cloud base. The cloud base heights varied between 700m and 110m throughout the 2¾ hour flight. Hasler et al. (1977a) developed an improved method for the verification of satellite-derived cloud motions using in situ wind measurements. Aircraft equipped with inertial navigation systems were used to determine the motion of selected tropical cumuli and to measure the environmental wind field. These results were compared with cloud motions derived from Synchronous Meteorological Satellite (SMS)

imagery. The magnitude of the vector difference between the aircraft-measured cloud motions and the ambient cloud base wind was $<1.3 msec^{-1}$ for 67% of the cases with track lengths ≥ 1 hour. These results were for long-lived maritime and undisturbed atmospheric conditions. Rodgers et al. (1978) compared cloud motions derived from SMS-2 and GOES-1 limited scan imagery on AOIPS and winds observed from NOAA research aircraft within the disturbed environments of hurricanes Eloise and Caroline. The results showed that the average drift in absolute speeds of winds by these two methods was approximately $2.5 msec^{-1}$ for both storms.

The objective of this paper is to examine the unique capabilities and inherent limitations of satellite-derived wind fields in describing the atmospheric conditions which precede and occur during severe local storm development. Six satellite image sets of wind vectors and their associated divergence fields are examined for the following time periods on 6 May 1975: 1758-1808 GMT, 1813-1823 GMT, 1828-1838 GMT, 1903-1913 GMT, 1918-1928 GMT, and 2002-2012 GMT. Five minute interval images are used to compute cloud velocities from image 1 to image 3 in the sequence (total period within each sequence: 10 minutes).

2. Wind Extraction Techniques

Wind extraction from cloud motions on geosynchronous satellite digital image data is performed on the Goddard Space Flight Center Atmospheric and Oceanographic Information Processing System (AOIPS). A computer graphics terminal, a joystick lever, and numerous function control switches permit interaction between the user, a television monitor, and a PDP 11/70 Processor (Billingsley, 1976). The cloud tracking is done using an interactive software system called the Meteorology Data Processing Package (METPAK). The METPAK directs several functions including landmark selection, navigation, and cloud top height measurement which allow the user to modify satellite digital image data.

a. Landmark Selection and Navigation

The navigation algorithm is adapted from the University of Wisconsin's McIDAS navigation model (Smith, 1975). The landmark selection and navigation functions provide the capability for

the transformation between image coordinates (line, pixel) and earth coordinates (latitude, longitude).

To determine navigation accuracy, a coordinate transformation technique is used to compute landmark residuals (Mottershead and Philips, 1976). The line (pixel) residuals are defined as the difference between the measured and recomputed image line (pixel) numbers of the landmarks. A landmark point is initially selected on the base image and automatically defined on the same point for every image in the sequence by shifting the images relative to the base image. Spin attitude and centering parameters are adjusted to make the calculated landmark positions agree with the initially measured landmark points. The navigation solution for the image sequences in this paper reproduced the landmark plane trajectory to within 0.00 ± 0.13 lines, 0.00 ± 0.15 pixels for the first landmark and 0.24 ± 0.39 lines, 1.97 ± 0.29 pixels for the second landmark. (The first group is the mean, and the second group is the standard deviation of the corresponding residuals.) In general, these residual statistics indicate an image alignment accurate to within 1 visible picture element or 1 km in earth location. The corresponding velocity resolution is $\leq 3 msec^{-1}$ for 5 minute interval images and $\leq 1.7 msec^{-1}$ for the vectors in the image 1 to image 3 sequence.

b. Cloud Top Height Measurement

A cloud top height algorithm developed by Mosher (Suomi, 1975) is used to differentiate between low, middle, and high clouds. Corrections are applied to the satellite viewing angles and solar zenith angles in the model. The physical thickness of the clouds and the number density of droplets are parameterized to determine the cloud's optical thickness. The optical thickness is used to calculate the infrared emissivity using Kirchoff's Law. Cloud top temperature is calculated using the emissivity and the percentage of cloud cover from the visible image. Finally, the cloud top height is determined from a standard atmosphere of temperature vs. height, corrected for latitude and date.

The absolute accuracy of this cloud top height algorithm has not been determined. Preliminary estimates by Smith (1975) have indicated an accuracy of ±50mb for low clouds. Errors are due to (1) an assumption that the clouds have no horizontal boundaries, (2) the utilization of ocean albedo values instead of land albedo values in the calculation of surface flux, and (3) the use of standard soundings instead of local soundings. An independent evaluation of the algorithm by Lo (1975) concluded that this method was the most efficient technique presently available for the purpose of estimating cloud top heights on the AOIPS. Lo stated two reasons for this conclusion: (1) the method was based on physical laws rather than statistics, and (2) the results were consistent with conventional measurements.

For this case study, selected low level cumuli have cloud top heights between 1.0km and 2.8km. It was assumed that clouds within this range would be moving at approximately the same level of flow. If the height difference between any two consecutive cloud top heights in the image sequence was $\geq$0.5km, the cloud was disregarded as an acceptable tracer.

c. Cloud Tracking

To measure cloud motion, a sequence of images is continuously time lapsed on a television monitor. Cloud displacement on successive images is divided by elapsed time to obtain velocity. Two methods of cloud tracking are available in the METPAK software: single pixel tracking and image correlation tracking. In single pixel tracking, a cursor defines the cloud location on successive images. The image coordinates are computed and a ground speed calculation is performed to obtain velocity. Either the brightness or geometric centroid of the cloud is chosen as the tracking point to decrease the influence of the cloud's own development or dissipation. In the image correlation mode, a "box" cursor surrounds the cloud area and an Euclidean Norm correlation is performed on adjacent pairs of areas. The coordinates of the best matching points are used as the coordinates of the tracer.

The cloud tracking in this study was done with the image correlation method. If the difference in magnitude between any two consecutive vectors in the image sequence was $>5msec^{-1}$,

the cloud was disregarded as an acceptable tracer. It was assumed that a cloud's motion would not change radically over 5 minute intervals.

3. Objective Analysis

The METPAK provides the capability to select an objective analysis function which produces interpolated wind fields and the kinematic parameters calculated from them for television display and film output. The current objective analysis is a modified Cressman (1959) technique which uses a circular weighting function to determine the value of the wind component at a grid point (Robinson and Gross, 1977). The weighting function consists of three factors: distance weighting, implicit axis proximity weighting, and shadowing. The distance weighting factor gives more importance to data which are located closer than farther away from a grid point. The implicit axis proximity factor gives more weight to data which are closer to a preferred axis. The shadowing factor assigns a smaller weighting value to a datum in the shadow of another measurement. The modified Cressman version includes an empirical adjustment process to provide for internal consistency in the data. In this case study, the interpolated u and v components are calculated at 0.3° grid point intervals and are used to derive divergence of the flow in spherical coordinates.

4. 6 May 1975 Case Study

On 6 May 1975, the immediate vicinity of an eastward moving dry line in the Central Plains became a highly preferred zone for thunderstorm development and squall line organization. Figure 1 shows an 1800 GMT satellite image of the two areas where clouds were tracked over sections of Nebraska, Iowa, Kansas, Missouri, Oklahoma, and Arkansas. Abundant low level moisture and dry air aloft coupled with a steep lapse rate created a potentially unstable atmosphere which displayed signs of convective development as early as 1600 GMT in South Dakota. By 2100 GMT, thunderstorm activity extended southward into eastern Texas.

A conventional meteorological analysis was performed to determine what conditions were present for severe local storm development. The analysis indicated favorable conditions for severe

weather. The 1200 GMT Omaha sounding showed a mean surface mixing ratio ($\overline{w}$) of 13g kg^{-1} and a $\overline{w}$ of 0.9g kg^{-1} at 700mb. The air was nearly saturated up to 800mb and very dry between 790mb and 550mb. The stability indices showed a moderate chance of severe weather: Showalter Index = -3, K Index = 10, and FM Index = -4.2. Figure 2 shows a 1200 GMT composite chart of the significant features influencing thunderstorm development ahead of the dry line.

A meteorological feature which appeared to influence the initiation of severe thunderstorms along the dry line at 1815 GMT in the Omaha region was the advection of a cloud system shaped like a comma which is usually associated with areas of positive vorticity advection at mid and upper tropospheric levels.[1] According to Miller, an important prerequisite for storm formation often is the development or advection of these cloud systems.

According to NOAA Storm Data and the National Severe Storm Forecast Center (NSSFC) SELS Log, there were 54 reports of severe weather between 1900 GMT and 0200 GMT ahead of the dry line: 11 tornadoes, 34 cases of $\geq 3/4''$ hail, and 9 cases of winds which had speeds >50 knots.

5. Results

a. Introduction

Cloud tracking was performed for two 500 x 500km^2 areas (Fig. 1) using 0.9km visible SMS-2 5 minute interval data. Area 1 includes southeastern Nebraska, southwestern Iowa, northeastern Kansas, and northwestern Missouri. Area 2 includes southeastern Kansas, eastern Oklahoma, southwestern Missouri, western Arkansas, and northeastern Texas. Five hail-producing (hail diameter $\geq 3/4''$) thunderstorms occurred within these areas: one event in Area 1 and 4 events in Area 2 between 1900 GMT and 2205 GMT.

1. Miller, Robert C., 1977: Personal communication.

Satellite-derived cloud velocities and associated divergence fields were computed for six time periods: 1758-1808 GMT, 1813-1823 GMT, 1828-1838 GMT, 1903-1913 GMT, 1918-1928 GMT, and 2002-2012 GMT. The divergence fields were superimposed on their respective satellite images. Since the objective analysis program performs contouring to the edges of the satellite images, contours are often created in vector-free areas. Low level cumulus clouds in Areas 1 and 2 were surrounded by cloud-free areas to the west behind the dry line and were obscured by middle and upper level clouds to the east. Contours of divergence were removed in these data-void areas to emphasize adequate vector density regions. Contours were also removed from areas where the vector density was less than 8 vectors per 1° latitude/longitude square.

b. Cloud Vector Statistics

The satellite-derived cloud vectors and cloud top heights appeared to be reasonable and consistent within the 12 data sets for both areas. A statistical summary of the cloud motion vectors is shown in Table 1. These data are summarized for number of tracked clouds, mean wind speeds and directions, and mean cloud top heights.

In general, the number of tracked low level cumuli decreases with time due to cumulus cloud vertical development and obscuration of the low level cloud tracers by middle and upper level clouds. The number of vectors decreases by 82% in Area 1 and by 53% in Area 2 over a two hour period. Cloud velocities are about 3msec^{-1} faster on the average in Area 1 than in Area 2. The clouds in Area 1 are initially small, low level cumuli which develop rapidly in extent over two hours. A hail-producing thunderstorm occurred in this area between 2030 GMT and 2130 GMT. In Area 2, major thunderstorms have already developed by 1800 GMT. Small, trackable low level cumuli are located south and east of these thunderstorms. They are fairly quiescent and do not develop into thunderstorms. Their cloud top heights are about 0.5km lower on the average than the heights in Area 1.

Table 1
Statistical Summary of Satellite-Derived Cloud Vectors

Area	Time (GMT)	Number of Vectors	$\overline{\text{Velocity}}$ ($msec^{-1}$)	$\overline{\text{Direction}}$ (°)	Mean Cloud Top Height (km)
1	1758–1808	137	12.2	204	2.0
1	1813–1823	82	12.8	201	2.0
1	1828–1838	100	12.1	197	2.1
1	1903–1913	75	12.4	196	2.1
1	1918–1928	67	12.1	201	2.2
1	2002–2012	24	12.4	193	2.2
2	1758–1808	167	10.2	210	1.4
2	1813–1823	204	9.9	207	1.7
2	1828–1838	160	9.5	204	1.6
2	1903–1913	103	9.5	207	1.7
2	1918–1928	94	8.8	204	1.6
2	2002–2012	77	8.4	210	1.8

$\overline{\text{Velocity}}$ (Area 1): $\sigma = .938$
$\overline{\text{Velocity}}$ (Area 2): $\sigma = .671$

Small differences between the maximum and minimum values of cloud speed and direction and cloud top height for the two hour period indicate consistency within the satellite-derived cloud vector data. If $\overline{V}_{max}$ is the maximum mean cloud speed and $\overline{V}_{min}$ is the minimum mean cloud speed then $\Delta\overline{V} = \overline{V}_{max} - \overline{V}_{min} = 0.7 msec^{-1}$ for Area 1. If $\overline{\alpha}_{max}$ is the maximum mean cloud direction and $\overline{\alpha}_{min}$ is the minimum mean cloud direction then $\Delta\overline{\alpha} = \overline{\alpha}_{max} - \overline{\alpha}_{min} = 11°$ for Area 1. Similarly, if $\overline{CTH}$ is mean cloud top height, then $\Delta\overline{CTH} = \overline{CTH}_{max} - \overline{CTH}_{min} = 0.2$ km for Area 1. For Area 2, $\Delta\overline{V} = 1.8 msec^{-1}$, $\Delta\overline{\alpha} = 6°$, and $\Delta\overline{CTH} = 0.4$km. Consistency within the cloud vector data is significant since the cloud vectors must be located at the same level to obtain a meaningful time history of kinematic parameters within each area.

A comparison was made between the cloud vectors and rawinsonde winds, which were acquired from the Atmospheric Variability Experiment (AVE) II, to determine a LBF for the cloud vectors. Thirteen cloud vectors were tracked within 1/2° radius of a rawinsonde station located at Topeka, Kansas (39.04°N, 95.38°W). There was a 45 minute time difference between the 1715 GMT rawinsonde sounding and the 1800 GMT satellite image used in the comparison.

Table 2 shows the comparison between the cloud vectors and the rawinsonde data at levels of 950mb, 925mb, 900mb, 875mb, and 850mb. Differences in velocity (both speed and direction) are calculated and mean differences are found for vectors which are located within 1/4° and 1/2° radius of the rawinsonde station.

The satellite derived cloud vectors appear to have a LBF between 925mb and 900mb. At 1/4° radius, the mean speed differences are smallest for the 950–925mb levels. However, the mean directional differences are very large there in comparison with the 900–875mb levels. Since the mean speed difference at 900mb is similar to the mean speed difference at 925mb and the mean directional difference is smallest for 900mb, the LBF is probably closest to 900mb. At 1/2° radius, the mean speed differences are similar between the 950–925mb levels and the 900mb level. The mean directional difference is again smallest at 900mb. Surface reports and sounding analyses

Table 2

Velocity Differences (ΔV) Between the 1715 GMT Rawinsonde Data and the 1800 GMT Satellite Cloud Vectors at Various Pressure Levels

Satellite Cloud Vector Number	Satellite-Derived Cloud Top Height (km)	$\Delta V_{950-SAT}$ (ms^{-1}, deg)	$\Delta V_{925-SAT}$ (ms^{-1}, deg)	$\Delta V_{900-SAT}$ (ms^{-1}, deg)	$\Delta V_{875-SAT}$ (ms^{-1}, deg)	$\Delta V_{850-SAT}$ (ms^{-1}, deg)
1*	1.9	1.1, 19°	0.1, 17°	1.5, 5°	3.4, 2°	1.4, 6°
2*	1.7	1.9, 13°	3.1, 13°	4.5, 1°	6.2, 6°	4.4, 10°
3*	1.9	5.2, 15°	5.2, 15°	6.6, 3°	8.5, 4°	6.5, 8°
4	1.6	0.4, 13°	0.8, 11°	2.2, 1°	4.1, 8°	2.1, 12°
5	1.7	4.7, 11°	3.5, 9°	2.1, 3°	0.2, 10°	2.2, 14°
6	1.7	7.3, 27°	6.1, 25°	4.7, 13°	2.8, 6°	4.8, 2°
7	1.9	5.2, 30°	4.0, 28°	2.6, 16°	0.7, 9°	2.6, 5°
8	1.7	3.6, 22°	2.4, 20°	1.0, 8°	0.9, 1°	1.1, 3°
9	1.6	4.4, 26°	3.2, 14°	1.8, 12°	0.1, 5°	1.9, 1°
10	1.8	4.1, 17°	5.3, 15°	6.7, 3°	8.6, 4°	6.6, 8°
11	1.7	4.7, 7°	5.9, 5°	7.3, 7°	9.2, 14°	7.2, 18°
12	1.8	1.6, 15°	2.8, 13°	4.2, 1°	6.1, 6°	4.1, 10°
13	2.0	1.1, 19°	0.1, 17°	1.5, 5°	3.4, 2°	1.4, 6°
Mean Difference Vectors 1–3		2.7, 16°	2.8, 15°	4.2, 3°	6.0, 4°	4.1, 8°
Mean Difference Vectors 1–13		3.5, 18°	3.3, 16°	3.6, 6°	4.2, 6°	3.6, 8°

*Vectors 1–3 are located within 1/4° radius of the rawinsonde station; vectors 4–13 are located between 1/4° and 1/2° radius.

place cloud bases between 925–900mb and the Hans–Suring formula for cloud base height [z = 220 (T – Td)] computes a cloud base height of 900mb. These results indicate that clouds appear to be moving at the velocity of the environmental wind at cloud base levels.

For this case study, an LBF of 900mb implies mean differences of 3.6msec^{-1} and 6° between the rawinsonde winds and the 13 cloud vectors. Hubert and Whitney (1971) found a median vector deviation of 4.6msec^{-1} between cloud motions and rawinsonde winds for 600 clouds. A larger sample of cloud vectors and rawinsonde winds is currently being examined on AOIPS to determine the similarity of the two methods (rawinsonde vs. satellite) in measuring atmospheric motions.

c. Time Sequence of Divergence (Convergence)

Figures 3–12 show the time sequence of cloud vectors for Area 1 and their associated divergence fields for the period 1758–1928 GMT. These fields are superimposed on the SMS-2 visible images for the same period. The arrows represent the cloud vectors which are used to derive the divergence fields. They are oriented in the direction of flow and their lengths are proportional to the magnitude of their speeds. The dashed lines are contour values of convergence; the smooth lines are contours of divergence. All contour values of divergence (convergence) have units of 10^{-6} sec^{-1}.

An examination of the time sequence of the divergence fields reveals a consistent pattern of convergence which is located ahead of the dry line. Table 3 shows how the absolute maximum value of the convergent pattern changes with time for Area 1. The maximum value of the convergence generally increases with time in the area of potential thunderstorm development and varies within the range of 10^{-5} sec^{-1} to 10^{-4} sec^{-1}. These values reflect the consistency in the convergent patterns over the 2 hour time period. According to Houghton (1977), similar convergence distributions were obtained for 6 May 1975 at selected periods using cloud tracking

Table 3
Maximum Value of the Convergence for Area 1 from 1758 GMT to 2012 GMT

Time (GMT)	Maximum Value of the Convergence ($\times 10^{-5}$ sec^{-1})
1758–1808	4.3
1813–1823	7.2
1828–1838	4.7
1903–1913	6.1
1918–1928	7.9
2002–2012	10.0

techniques on the McIDAS facility at the University of Wisconsin.[2] This result shows that similar cloud vectors can be acquired from satellite data by two independent groups.

One should exercise caution in interpreting convergence patterns from wind vectors when thunderstorms exist in the cloud tracking areas. Data-void areas are created in the vector field since thunderstorm anvils obscure the lower level clouds. This situation becomes critical in Area 1 with the development of a hail-producing thunderstorm cell after 2000 GMT. Convergence patterns for 2002 GMT, Area 1 and Area 2 are not shown because thunderstorms created critical data-void areas in the low level vector field. An ideal situation would be to acquire as many in situ wind measurements from aircraft flights to determine the wind field within the immediate vicinity of a thunderstorm cell. Since this situation is usually infeasible, the problem of data-void areas will be best eliminated by limiting cloud tracking in large areas to the time period preceding thunderstorm anvil expansion.

2. Houghton, David, 1977: Personal communication.

d. Combined Rawinsonde and Satellite-Derived Divergence

A divergence field was recalculated for the 1758-1808 GMT time period using the cloud vectors and the 1800 GMT rawinsonde wind vector for Topeka, Kansas. Figure 13 shows the location of this point (marked by an x) and the recalculated divergence field. This divergence field was calculated using the original objective analysis parameters and was found to be similar to the original convergence pattern in Figure 3. The position of the patterns remained the same and the magnitudes were only slightly different in the value of the maximum convergence. The original value of the maximum convergence was -4.3×10^{-5} sec^{-1} while the recalculated value was -5.0×10^{-5} sec^{-1}.

The inclusion of one rawinsonde wind did not greatly affect the distribution of divergence patterns. Since the measurements of divergence are sensitive to small differences of wind speed and direction, it is important to test the sensitivity of these fields to the addition and deletion of wind vectors. Future case studies will incorporate a larger combined sample of rawinsonde and satellite-derived winds to determine how much these fields will change under various conditions.

e. Effect of Random Errors on the Cloud Fields

Hasler and Rodgers (1977b) have developed a technique to measure the effect of random errors on the cloud vectors and associated kinematic parameters using a Monte Carlo error analysis. A normally distributed error with a standard deviation which may be varied is applied to the start and end coordinates of each cloud vector by a random number generator. The unperturbed and perturbed cloud vectors are subtracted to determine the effect of the errors on the cloud velocity and associated kinematic parameters. This technique evaluates the effects of time interval, image resolution, grid spacing and degree of smoothing. It can not evaluate systematic errors due to selection of cloud vectors not representative of a selected level.

Hasler applied this technique to 81 low level cloud vectors which were tracked for the 1813–1823 GMT time period on 6 May 1975.[3] These vectors were independently remeasured and the magnitude of the vector difference (MVD) was computed between the original and remeasured vectors. These MVD's were ranked and the 67% largest were determined. The repeatability error was very small: $|\vec{V} - \vec{V}_{remeasured}|_{67\%} = .15 msec^{-1}$. The start and end coordinates of the original vectors were perturbed with a $\sigma = 1.0$ pixel and 2/3rd's of the differences between the original and perturbed vectors were equal to or less than $2.3 msec^{-1}$ ($|\vec{V} - \vec{V}_{perturbed}|_{67\%} = 2.3 msec^{-1}$). The perturbed and unperturbed cloud vectors were then interpolated to uniform grid points using the Cressman (1959) technique. The difference between the unperturbed and perturbed analyzed wind fields resulted in a random error of $|\vec{V} - \vec{V}_{perturbed}|_{67\%} = 1.4 msec^{-1}$. When the unperturbed and perturbed divergence fields were subtracted from each other, $|DIV - DIV_{perturbed}|_{67\%} = 4.4 \times 10^{-6}$ sec^{-1}. This result is only 7% of the maximum value of the unperturbed field and implies that contours greater than 4.4×10^{-6} sec^{-1} have significance at the 67% level or better.

The above results indicate that random errors of 0.6 x image resolution ÷ total time interval can be expected in the initial cloud vectors. The random error of $2.3 msec^{-1}$ in the initial vectors can be improved to $1.4 msec^{-1}$ by performing an objective analysis of the wind field. This improvement is possible since random errors cancel each other when more than one vector contributes to the wind at a grid point. The cloud vectors in this specific time period appear to be acceptable to infer the ambient wind field. Additional error analyses will be done to determine random errors in other cloud vector sets.

3. Hasler, Fritz A., 1978: Personal communication.

f. Impact of Longer Image Intervals on Cloud Tracking Severe Local Storm Events

A brief study was done on the impact of using satellite data with different image intervals for cloud tracking in severe local storms. Table 4 shows the number of acceptable cloud tracers for Area 1 at 5, 10, and 15 minute intervals. An attempt was made in the comparison to use satellite images which were very close in time to avoid changes in the cloud field due to substantial cloud growth. Similar cloud tracking techniques were utilized for all three sets.

The comparison shows that frequent interval satellite data are necessary to acquire reasonable cloud vector fields in a severe local storm situation. There was a 69% reduction in the number of tracers at 10 minute intervals and a 98% reduction at 15 minute intervals. Many cloud elements disappeared after 10 or 15 minutes or grew too large to be considered acceptable low level wind tracers. Smaller time intervals ($\leq$5 minutes) allowed the continuous recognition of specific, rapidly-changing cumulus tracers. Additional case studies will be done to determine whether these percentages are unique or average values for cloud tracking severe local storm events.

6. Summary

An examination of frequent interval satellite digital image data demonstrates the feasibility of using satellite-derived cloud vectors in conjunction with conventional wind data to describe mesoscale features which are connected to severe local storm events. These features in the

Table 4
Number of Cloud Tracers for Varied Image Intervals

Time Interval (Minutes)	Image Sequence Period (GMT)	Number of Low Level Cloud Tracers
5	1758-1803-1808	137
10	1808-1818-1828	42
15	1758-1813-1828	3

atmospheric flow appear to be related to the subsequent occurrence of severe weather. Satellite-derived cloud vector fields are extremely consistent and approximately represent the ambient wind when they are placed at their correct level in the atmosphere. For this case study, a significant feature, which is revealed by the satellite-derived cloud vectors, is a consistent pattern of convergence located ahead of a dry line — a preferential area for strong convective activity. Satellite-derived cloud vectors can probably be used to localize areas of mesoscale convergence before the appearance of thunderstorm cells. These cloud vectors will certainly need to be acquired using very frequent interval satellite images preferably at less than or equal to 5 minute intervals.

There is enormous potential in these wind extraction techniques to improve real-time forecasting of severe local storms. One of the current limitations in the operational synoptic network is the lack of winds to describe the basic kinematics of severe local storm environments. With improvements in the assignment of levels to the satellite-derived cloud vectors and the adjustment of satellite "winds" to conventional wind levels, an increased application of combined satellite and conventional data can advance our lead-time in forecasting the occurrence of severe weather.

References

Billingsley, J. B., 1976: Interaction image processing for meteorological applications at NASA/GSFC. Preprints 7th Conf. on Aerospace and Aeronautical Meteorology and Symposium on Remote Sensing from Satellites, Melbourne, Amer. Meteor. Soc., 268-275.

Fujita, T. T., E. W. Pearl and W. E. Shenk, 1975: Satellite-tracked cumulus velocities. J. Appl. Meteor., 14, 407-413.

Hasler, A. F., W. E. Shenk and W. C. Skillman, 1977a: Wind estimates from cloud motions: Results from phases I, II, and III of an in situ aircraft verification experiment. J. Appl. Meteor., 16, 812-815.

_____, and E. B. Rodgers, 1977b: An error analysis of tropical cyclone divergence and vorticity fields derived from satellite cloud winds on the Atmospheric and Oceanographic Information Processing System (AOIPS). Preprints 11th Tech. Conf. on Hurricanes and Tropical Meteorology, Miami Beach, Amer. Meteor. Soc., 670-675.

Hubert, L., and L. Whitney, 1971: Wind estimation from geostationary satellite pictures. Mon. Wea. Rev., 99, 665-672.

Lo, R. C., 1975: An evaluation of the University of Wisconsin McIDAS cloud height (CLDHGT) program. Computer Sciences Corp., NASA Contract Rep. NAS-11999, Task Assignment 619, 11 pp.

Mottershead, C. T., and D. R. Philips, 1976: Image navigation for geosynchronous meteorological satellites. Preprints 7th Conf. on Aerospace and Aeronautical Meteorology and Symposium on Remote Sensing from Satellites, Melbourne, Amer. Meteor. Soc., 260-264.

Robinson, H., and W. Gross, 1977: Survey of three-dimensional objective analyses. Computer Sciences Corp., NASA Contract NAS5-11999, Task Assignment 875, 46 pp.

Rodgers, E. B., R. C. Gentry, W. Shenk and V. Oliver, 1978: The benefits of using short interval satellite images to derive winds for tropical cyclones. NASA TM 79594, 32 pp.

Smith, E. A., 1975: The McIDAS system. IEEE. Trans. Geosci. Electr., GE-13, No. 3, 123-136.

Suomi, V. E., 1975: Man computer interactive data access system (McIDAS). NASA Contract NAS5-23296, University of Wisconsin, Madison.

Wagner, P. B., and J. W. Telford, 1976: The measurement of air motion in and near clouds. Preprints International Cloud Physics Conf., Boulder, Amer. Meteor. Soc., 669-672.

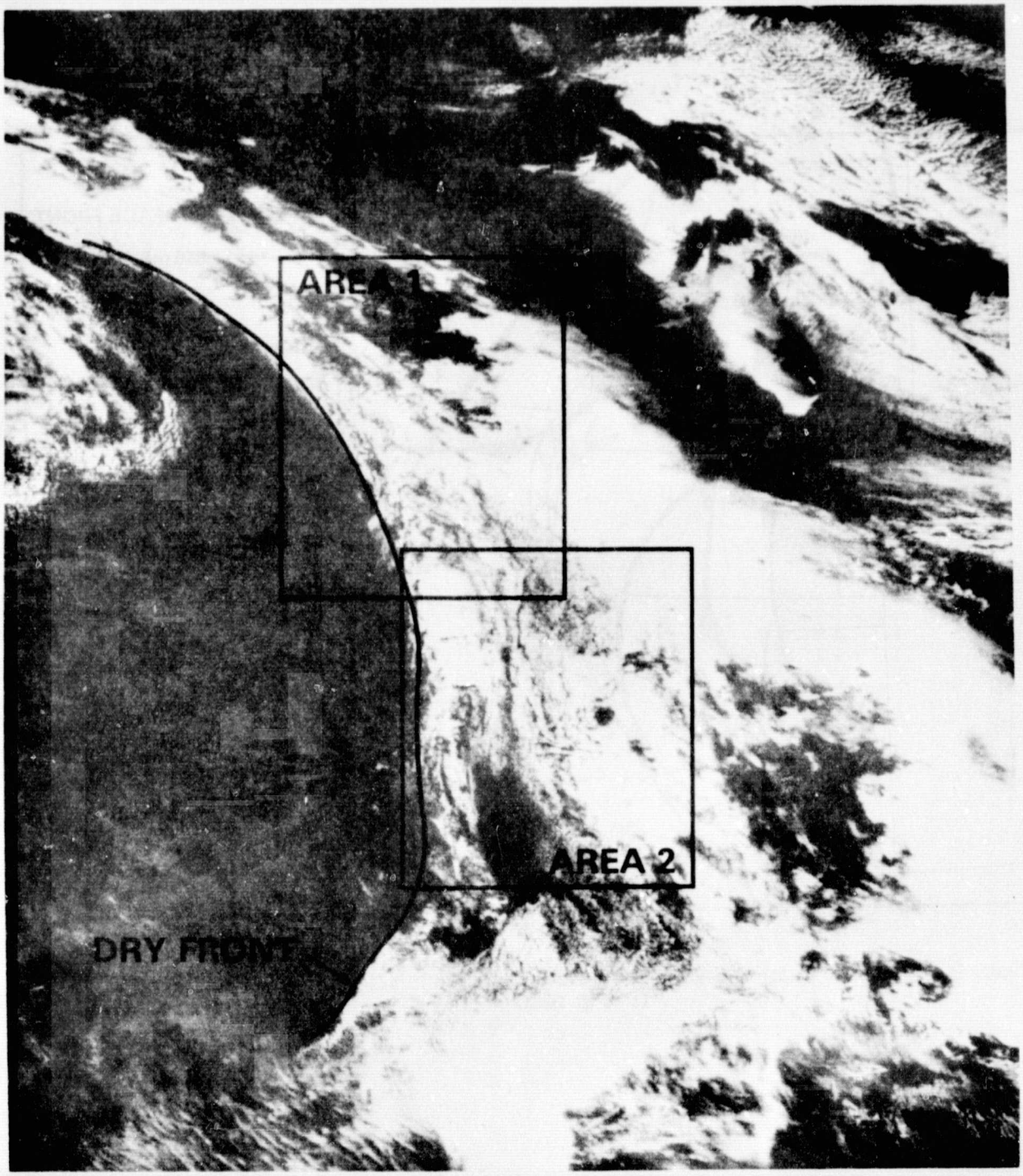

Figure 1. Cloud Tracking Areas for 6 May 1975

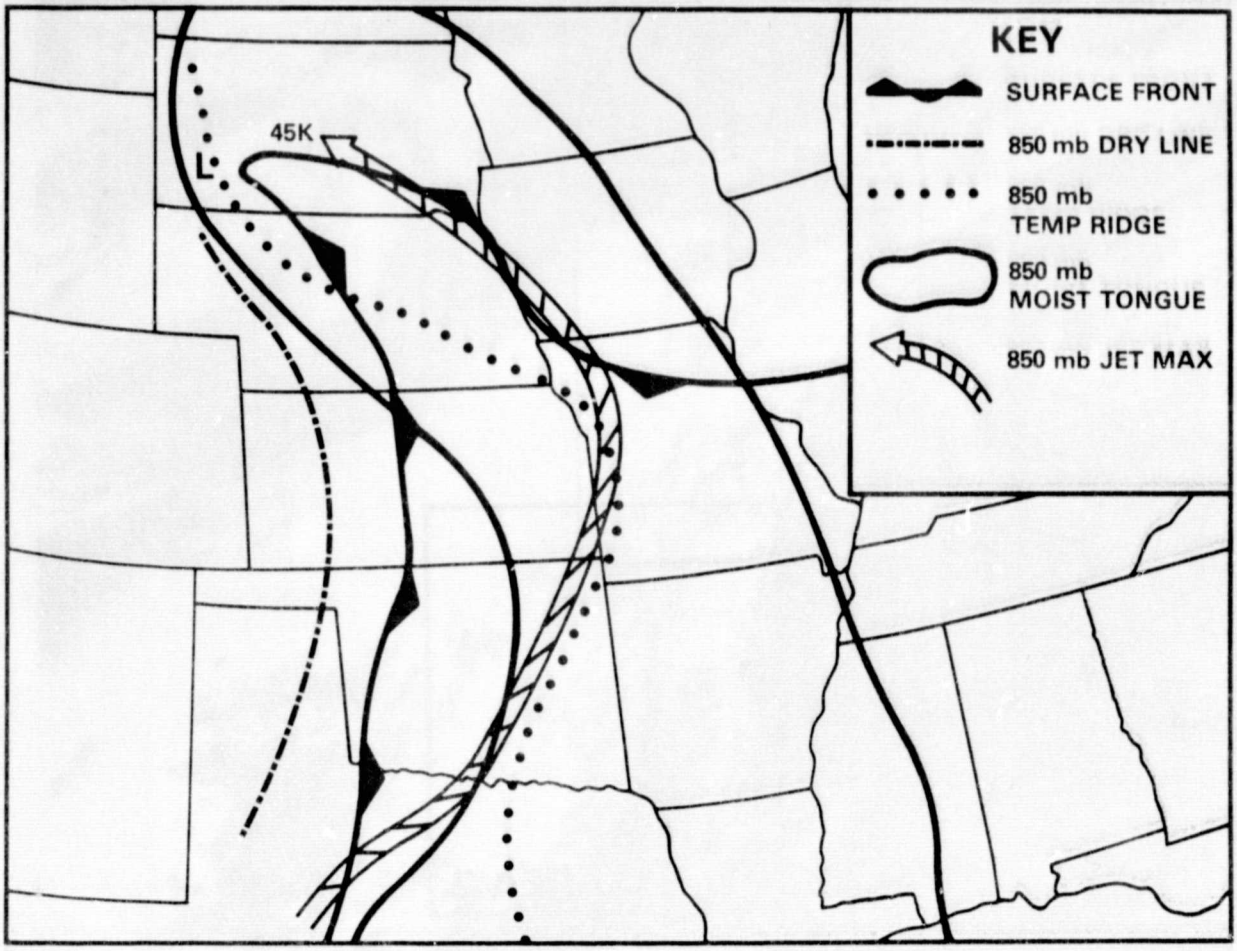

Figure 2. Composite Chart of Significant Surface and 850mb Meteorological Features for 6 May 1975 at 1200 GMT

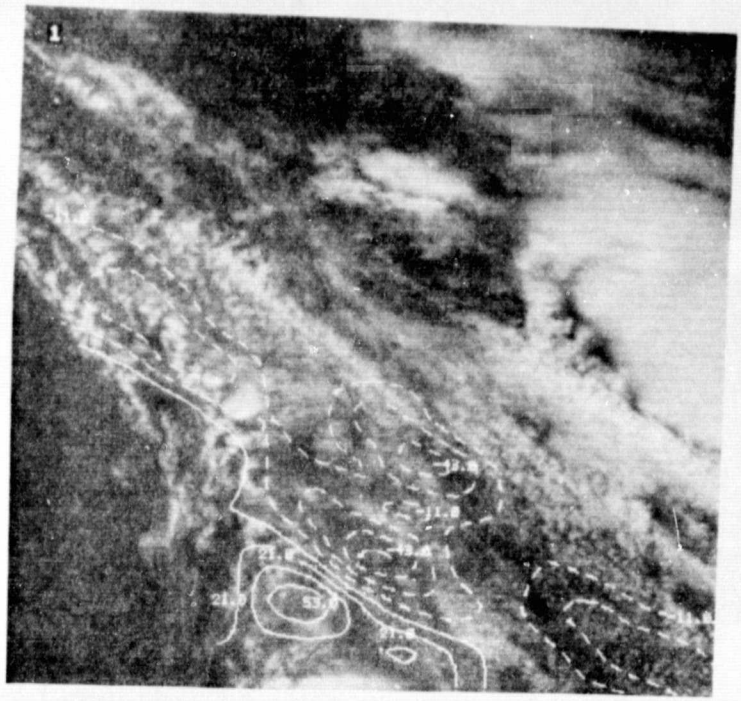

Figure 3. Divergence Field (x 10^{-6} sec^{-1}) for 1758–1808 GMT, Area 1

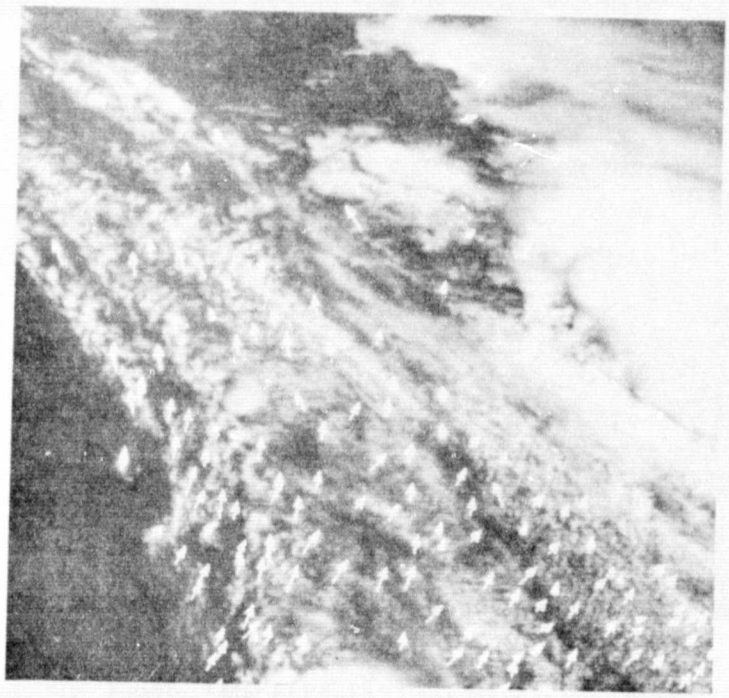

Figure 4. Cloud Vector Field for 1758–1808 GMT, Area 1

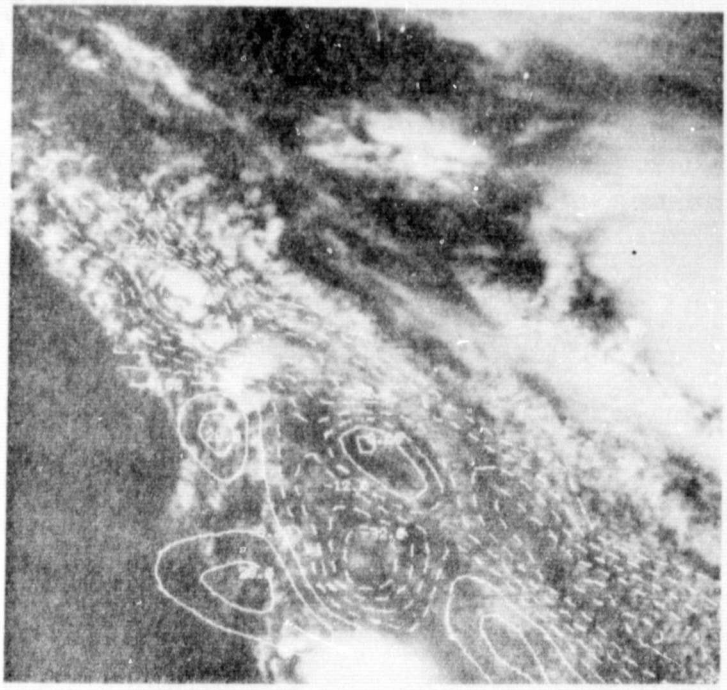

Figure 5. Divergence Field (x 10^{-6} sec^{-1}) for 1813–1823 GMT, Area 1

Figure 6. Cloud Vector Field for 1813–1823 GMT, Area 1

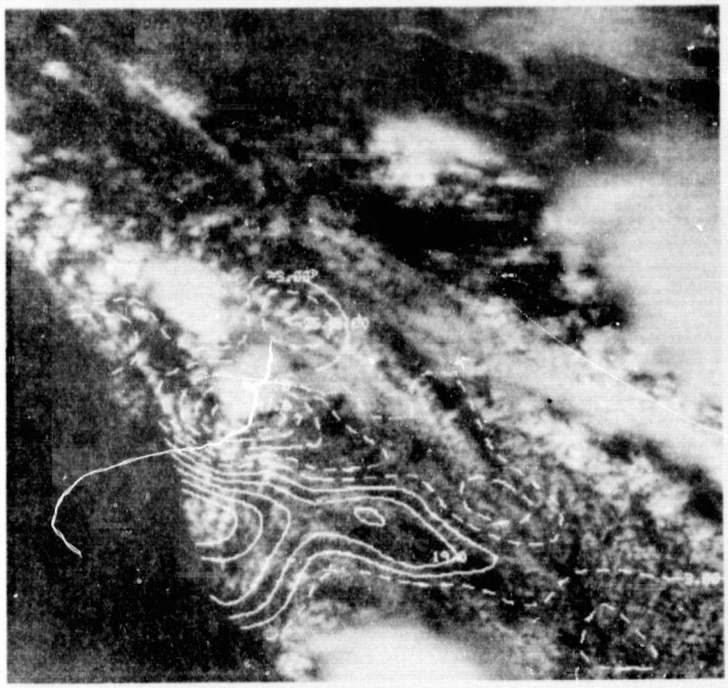

Figure 7. Divergence Field (x 10^{-6} sec^{-1}) for 1828-1838 GMT, Area 1

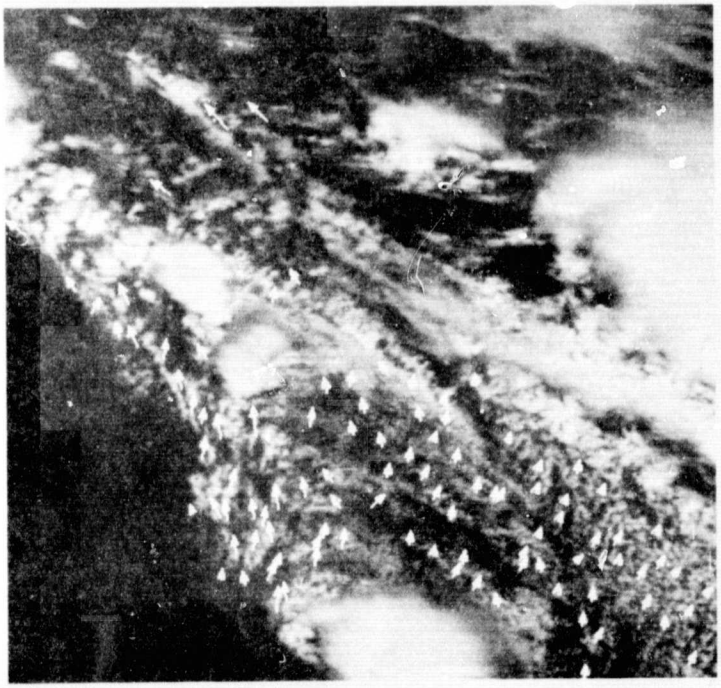

Figure 8. Cloud Vector Field for 1828-1838 GMT, Area 1

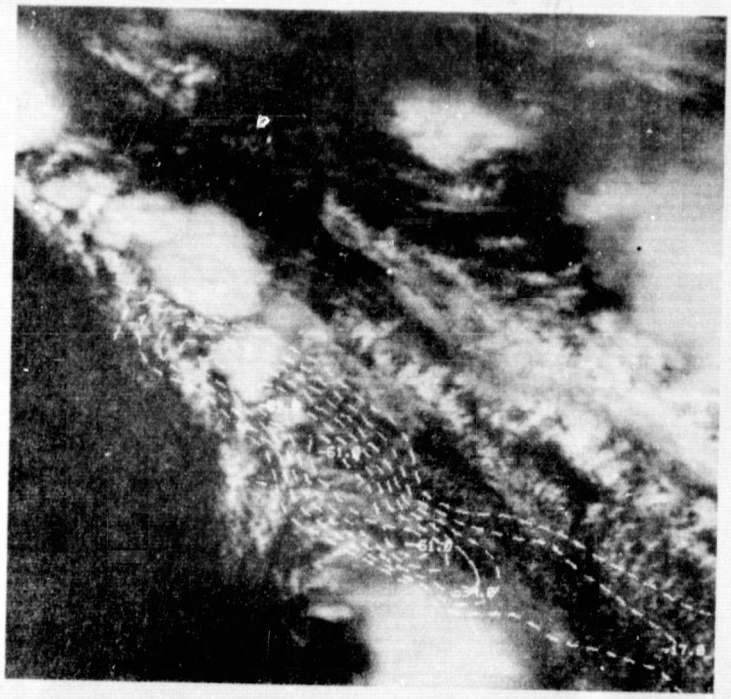

Figure 9. Divergence Field (x 10^{-6} sec^{-1}) for 1903-1913 GMT, Area 1

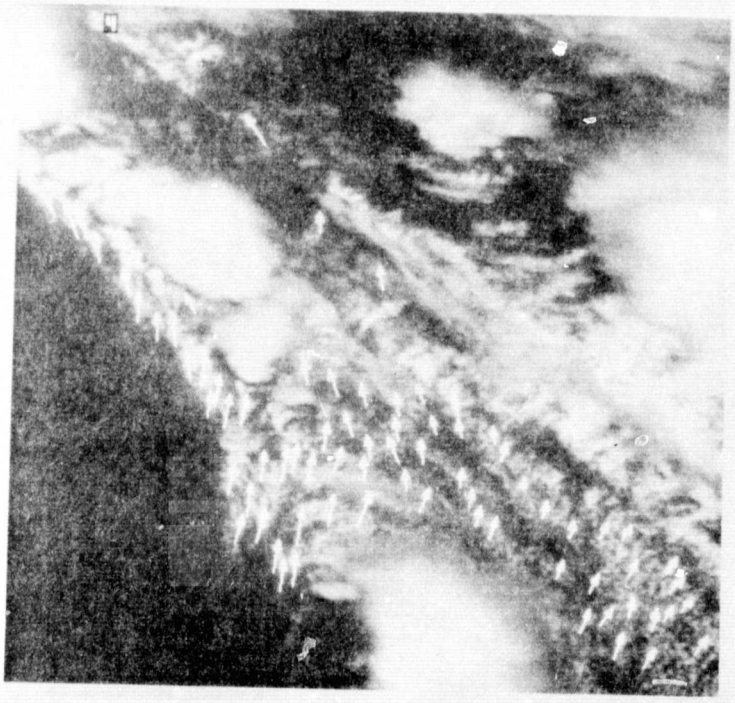

Figure 10. Cloud Vector Field for 1903-1913 GMT, Area 1

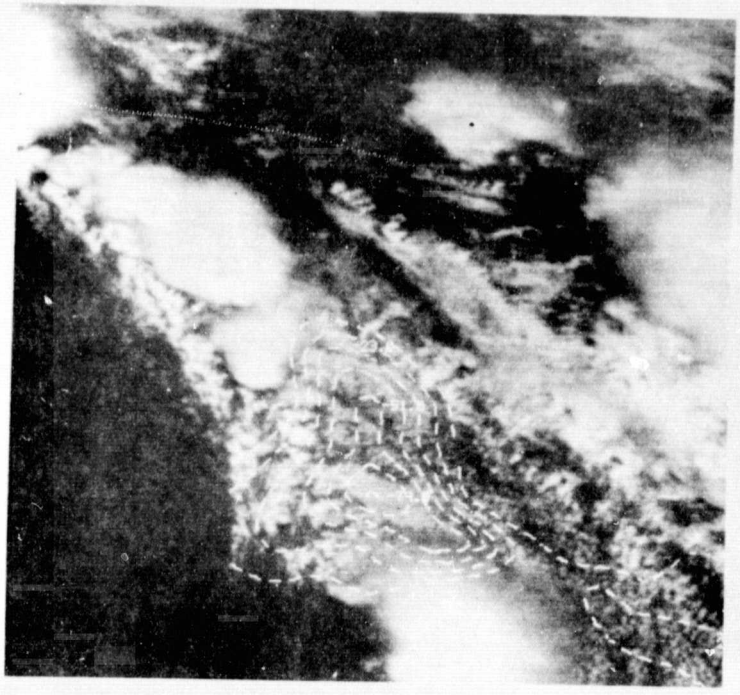

Figure 11. Divergence Field (x 10^{-6} sec^{-1}) for 1918-1928 GMT, Area 1

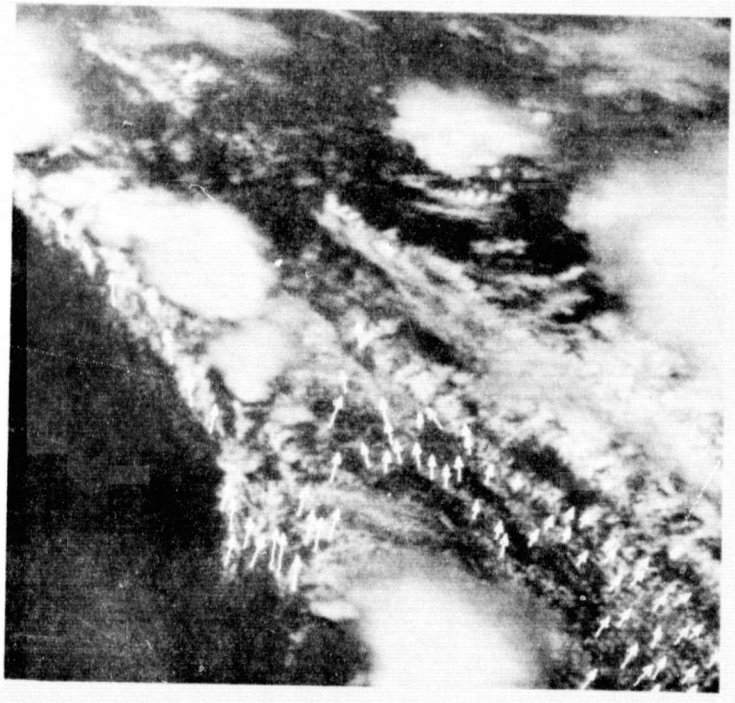

Figure 12. Cloud Vector Field for 1918-1928 GMT, Area 1

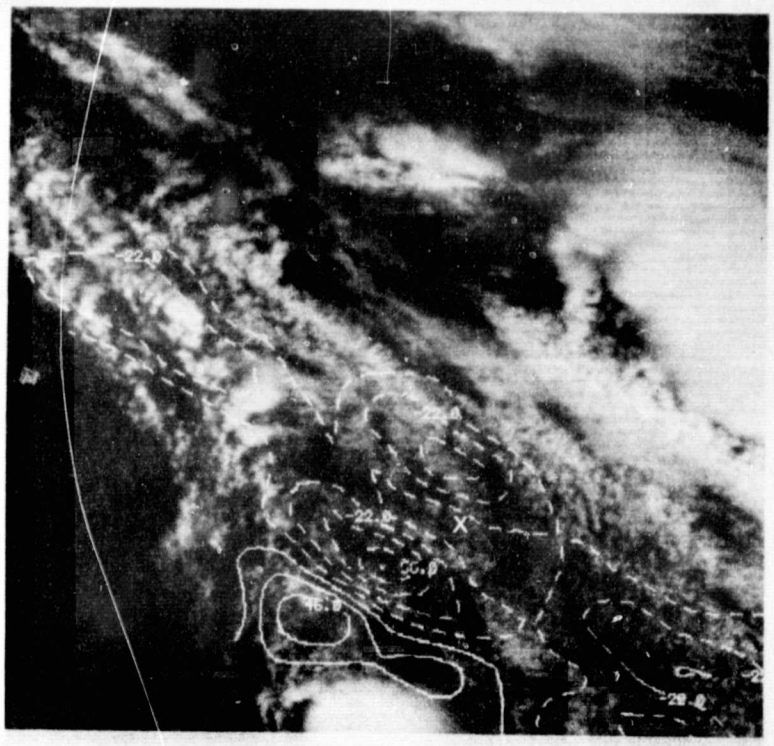

Figure 13. Divergence Field (x 10^{-6} sec^{-1}) for the Combined Cloud Vectors and Rawinsonde Wind at 1758-1808 GMT

FIGURE CAPTIONS

Figure 1. Cloud Tracking Areas for 6 May 1975

Figure 2. Composite Chart of Significant Surface and 850mb Meteorological Features for 6 May 1975 at 1200 GMT

Figure 3. Divergence Field (x 10^{-6} sec^{-1}) for 1758–1808 GMT, Area 1

Figure 4. Cloud Vector Field for 1758–1808 GMT, Area 1

Figure 5. Divergence Field (x 10^{-6} sec^{-1}) for 1813–1823 GMT, Area 1

Figure 6. Cloud Vector Field for 1813–1823 GMT, Area 1

Figure 7. Divergence Field (x 10^{-6} sec^{-1}) for 1828–1838 GMT, Area 1

Figure 8. Cloud Vector Field for 1828–1838 GMT, Area 1

Figure 9. Divergence Field (x 10^{-6} sec^{-1}) for 1903–1913 GMT, Area 1

Figure 10. Cloud Vector Field for 1903–1913 GMT, Area 1

Figure 11. Divergence Field (x 10^{-6} sec^{-1}) for 1918–1928 GMT, Area 1

Figure 12. Cloud Vector Field for 1918–1928 GMT, Area 1

Figure 13. Divergence Field (x 10^{-6} sec^{-1}) for the Combined Cloud Vectors and Rawinsonde Wind at 1758–1808 GMT

TABLES